J. Fluid Mech. (2009), *vol.* 618, *pp.* 243–261.
doi:10.1017/S0022112008004114 Printed in the United Kingdom

Short-time self-diffusion of nearly hard spheres at an oil–water interface

Y. PENG[1], W. CHEN[1], TH. M. FISCHER[2], D. A. WEITZ[3] AND P. TONG[1]†

[1]Department of Physics, Hong Kong University of Science and Technology, Clear Water Bay, Kowloon, Hong Kong

[2]Institute of Experimental Physics V, University of Bayreuth, 95440 Bayreuth, Germany

[3]Department of Physics and School of Engineering and Applied Sciences, Harvard University, Cambridge, MA 02138, USA

(Received 17 February 2008 and in revised form 2 September 2008)

Optical microscopy and multi-particle tracking are used to study hydrodynamic interactions of monodisperse polymethylmethacrylate (PMMA) spheres at a decalin–water interface. The short-time self-diffusion coefficient measured at low surface coverage has the form $D_S^S(n) = \alpha D_0(1 - \beta n)$, where n is the area fraction occupied by the particles, and D_0 is the Stokes–Einstein diffusion coefficient in the bulk suspension of PMMA spheres in decalin. The measured values of α are found to be in good agreement with the numerical calculation for the drag coefficient of interfacial particles. The measured values of β differ from that obtained for bulk suspensions, indicating that hydrodynamic interactions between the particles have interesting new features at the interface.

1. Introduction

The study of structures and dynamics of macromolecules and colloids at liquid–liquid or liquid–air interfaces is of fundamental interest for our general understanding of two-dimensional soft-matter systems; it also has immense practical applications in catalysis, material synthesis, microfluidics and nanotechnology (Helmer 2005). For example it is essential for optimizing the behaviour of solid-stabilized emulsion (Binks 1998; Dinsmore *et al.* 2002). Moreover, the study of interfacial dynamics and interactions is inherently connected to cell biology. Many biochemical reactions and intracellular signalling that sustain life occur at interfaces. For example diffusive transport of lipids and membrane-bound proteins plays an important role in many aspects of cell biology (Sackmann 1996; Dahan *et al.* 2003). For these reasons, the past decade has seen a growing interest in the use of the unique environment of interfaces to explore fascinating science and new applications. A monolayer of colloidal particles suspended at an oil–water (or water–air) interface has served as a model system to study a range of important issues at soft interfaces. Examples include two-dimensional ordering (Onada 1985), crystallization (Pieranski 1980) and diffusion-limited aggregation (Hurd & Shaefer 1985), interactions between similarly charged particles (Nikolaides *et al.* 2002; Chen *et al.* 2005) and dislocation boundaries

† Email address for correspondence: penger@ust.hk

of a colloidal crystal ball (Bausch *et al.* 2002; Lipowsky *et al.* 2005). These studies have focused on the equilibrium properties of the interfacial particles.

Colloidal particles have also been used as tracer particles to study the rheological properties of soft interfaces. For example Sickert and Rondelez (2003) measured the Brownian diffusion coefficient of 0.4 μm diameter polystyrene beads immersed in a monolayer of surfactant molecules at a water–air interface. Prasad, Koehler & Weeks (2006) extended the single-particle method to two-particle microrheology by measuring the relative diffusion between two micron-sized polystyrene beads suspended at a protein-coated water–air interface. While these measurements revealed interesting new features of tracer diffusion in macromolecular films, interpretation of the experimental results is not straightforward (Fischer 2004; Sickert & Rondelez 2004; Sickert, Rondelez & Stone 2007). The measured diffusion coefficient is inversely proportional to the drag coefficient felt by the interfacial particles. The theoretical calculations, which connect the measured drag coefficient to the surface rheological properties of interest, such as the surface shear viscosity η_s, consider idealized situations, whereas the actual systems used in the experiment often reveal interesting but unexpected deviations.

It is known that the drag coefficient of the interfacial particles is very sensitive to the detailed geometry of the particles and the interface involved and also to the boundary conditions at the interface. In considering the diffusion of proteins and other membrane-bound particles in biological or artificial membranes, Saffman's model (Saffman & Delbrück 1975; Saffman 1976) and later extensions (Stone & Ajdari 1998) treat the tracer particle as a thin cylindrical disk with the same height as that of the membrane (a thin viscous layer of viscosity η_s) overlaying a much thicker fluid layer of viscosity η. The actual tracer particles used in the above experiments (Sickert & Rondelez 2003; Prasad *et al.* 2006), however, are of the order of sub-micrometres in diameter, which is more than 1000 times larger than the thickness of the surfactant monolayer (or bilayer). When considering the motion of tracer spheres in a viscous monolayer or membrane on one fluid, or between two infinitely thick viscous fluids, two different boundary conditions at the interface were employed. Radoev, Nedjalkov & Djakovich (1992) and Danov *et al.* (1995) assumed the interface to be free of viscous stress (hence having constant surface pressure) and neglected the Marangoni effect due to surfactant-density gradients at the interface. In recent calculations, Fischer, Dhar & Heinig (2006) and Stone (Sickert, Rondelez & Stone, 2007) noted that Marangoni forces are important even when the surfactant concentration at the interface is low. They obtained analytical and numerical results for the viscous drag of tracer spheres with the boundary condition that the interface be incompressible.

Compared to the large number of theoretical investigations, systematic experimental studies of colloidal diffusion at interfaces are scarce. The lack of progress is partially due to a lack of well-controlled two-dimensional colloidal systems for the experimental studies. On the contrary, many model colloidal suspensions have been developed for the study of colloidal dynamics in three dimensions (Pusey 1991). Early experiments on colloidal diffusion at liquid–liquid (or liquid–air) interfaces (Radoev *et al.* 1992; Sickert & Rondelez 2003) were carried out only for a few particles. Because of the limited statistics, the measured diffusion coefficient suffered large experimental uncertainties, making it difficult to quantitatively compare with the theoretical predictions (Sickert & Rondelez 2003, 2004; Fischer 2004). The interactions and dynamics of colloidal particles are known to be sensitive to weak forces (of order pico- or femto-Newtons). This sensitivity is further magnified at interfaces. As a result, the stability of interfacial particles becomes extremely sensitive to impurities

at the interface (Fernández-Toledano *et al.* 2004). Accurate measurements of particle motion require well-controlled procedures to thoroughly clean the interface and colloidal samples, so that a well-dispersed monolayer of particles can be routinely made at the interface. Unstable particles form colloidal aggregates or clusters at the interface, making the measurement of individual particle motion inaccurate or impossible if there are too many colloidal aggregates present in the sample. In a recent experiment, Chen *et al.* (2006) developed the experimental procedures necessary to produce such a monolayer of colloidal particles. With the well-controlled two-dimensional colloidal systems, one can carry out precise measurements of the particles' diffusion coefficient at different interfaces. Such measurements are needed to verify the theoretical calculations for interfacial diffusion at interfaces with (Dimova *et al.* 2000; Fischer *et al.* 2006) and without (Radoev *et al.* 1992; Danov *et al.* 1995; Fischer *et al.* 2006) a surfactant monolayer and at biological membranes (Saffman & Delbrück 1975; Saffman 1976; Stone & Ajdari 1998). These theoretical calculations used similar continuum equations of motion but made different assumptions about the boundary conditions at the interface and between the tracer particles and the interface.

In this paper, we report results of a systematic study of short-time self-diffusion of monodisperse polymethylmethacrylate (PMMA) spheres at a decalin–water interface. As will be shown later, this is an interesting colloidal system in which the hydrodynamic interactions between the particles are three-dimensional, involving both the interface and the upper and lower fluid phases. Because the colloidal system is two-dimensional without influence of gravity and clearly visible without multiple scattering, precise measurements of particle's diffusion coefficient and pair correlation function $g(r)$ can be carried out conveniently using optical microscopy and particle-tracking techniques. All these advantages make the two-dimensional monolayer of PMMA particles a unique and ideal system to study the interfacial hydrodynamics and rheology of soft interfaces. In the experiment, we measure the mean squared displacement (MSD)

$$\langle \Delta \boldsymbol{r}^2(\tau) \rangle = (1/N) \sum_i \langle |\boldsymbol{r}_i(t+\tau) - \boldsymbol{r}_i(t)|^2 \rangle_t \tag{1.1}$$

of a diffusing particle as a function of lag time τ, where $\boldsymbol{r}_i(t)$ is the position of the ith particle at time t; N is the number of particles included in the calculation; and the angle brackets $\langle \ldots \rangle_t$ indicate an average over t.

The diffusion of interfacial particles is characterized by two distinct time regimes. For low surface coverage and times much less than the time $t_0 = (2a)^2/D_0$ for a particle to diffuse over its own diameter $d = 2a$, the particle's motion is not hindered by direct interactions with neighbouring particles, and only the hydrodynamic interactions with the surrounding fluid are important. Here $D_0 = k_B T/(6\pi\eta a)$ is the Stokes–Einstein diffusion coefficient for a single particle with thermal energy $k_B T$, fully immersed in a liquid of viscosity η. At long times ($\tau \gg t_0$), however, the particle's motion is impeded by direct interactions with neighbouring particles, and thus the self-diffusion is affected by both direct and hydrodynamic interactions. While the above arguments were given originally for three-dimensional colloidal diffusion (Qiu *et al.* 1990; Van Blaaderen *et al.* 1992; Segre, Behrend & Pusey 1995), we expect this is also true for interfacial diffusion.

Previous work (Zahn, Mendez-Alcaraz & Maret 1997; Rinn *et al.* 1999; Kollmann *et al.* 2002) reported the measurements of the long-time self-diffusion coefficient D_S^L for large paramagnetic latex spheres at a water-air interface. Because of long-range

Sample	d (μm) (±5%)	D_0 (μm^2 s^{-1})	α (±7%)	β (±10%)
PMMA1	1.19	0.145	0.97	1.4 (1.2)
PMMA2	0.66	0.260	1.04	2.8

TABLE 1. Particle samples used in the experiment and the fitted values of α and β from the measured short-time self-diffusion coefficient $D_S^S = \alpha D_0(1-\beta n)$. The numbers in the parentheses are obtained from a second-order polynomial fit (see text).

direct interactions, the interpretation of the measurements is complicated by a combination of structural and hydrodynamic effects. In this paper we focus on new measurements of the short-time self-diffusion coefficient $D_S^S(n)$ as a function of the area fraction, $n = \pi a^2 \aleph / A$, occupied by the interfacial particles. Here $\aleph$ is the total number of particles in the area A. The measured $D_S^S(n)$ is directly related to the drag coefficient ξ of the tracer particles at the interface, and the results will be compared with the numerically calculated ξ.

The remainder of the paper is organized as follows. We first describe the apparatus and the experimental method in § 2. Diffusion measurements are presented in § 3, and further discussions are given § 4. Finally, the work is summarized in § 5.

2. Experiment

The particles used in the experiment are PMMA spheres synthesized by Andrew Schofield of University of Edinburgh (Schofield 2007). The PMMA spheres have a poly(hydroxystearic acid) (PHSA) stabilizing layer ~10 nm in thickness, which is grafted to the particle surface to provide steric stabilization in non-polar solvents (Antl *et al.* 1986). They have been widely used as a model hard-sphere system to study the equilibrium and dynamic properties of bulk colloidal suspensions (Pusey 1991). Two particle sizes are used in the experiment: one has diameter $d = 2a = 1.19\,\mu$m (PMMA1) and the other has $d = 0.66\,\mu$m (PMMA2). Both particles are uniform in size distribution, with polydispersity less than 5%. They have a density of 1.19 g cm^{-13} and a refractive index of 1.49. The particles are thoroughly cleaned via multiple cycles (typically 5 times) of centrifugation, removing impurities, and are resuspended in clean decahydronaphthalene (decalin), used as received. The solvent decalin (a mixture of cis and trans with density 0.89 g cm^{-13}) was purchased from Acros Organics. Using a falling ball viscometer (Gilmont Instruments), we measure the viscosity of the decalin to be $\eta_d = 2.5$ cP at 22.5°C. Dynamic light scattering (Berne & Pecora 1976) is used to measure the diffusion coefficient D_0 of the individual PMMA particles in a dilute suspension in decalin. Using the Stokes–Einstein relationship $D_0 = k_B T/(3\pi\eta_d d)$ with the measured decalin viscosity η_d, we also obtain the particle diameter d. Table 1 gives the measured values of d and D_0 for the two particle samples.

The water–decalin interface is prepared using a sample cell shown in figure 1(*a*). The sample cell is made of stainless steel (which is hydrophilic) with two concentric and disk-shaped containers. The outer container has inner diameter 40 mm and height 4 mm. The inner container has inner diameter 22 mm and height 1.6 mm. There are four holes in the inner container, which are cylindrical in shape, with diameter 4–6 mm and height 0.8 mm. These four holes serve as four independent sample cells for the diffusion measurements to be discussed later. The bottom of each hole is sealed with a 0.1 mm thick glass cover slip, which also serves as an optical window. Because the density of water is larger than that of decalin, we first fill the holes to the top

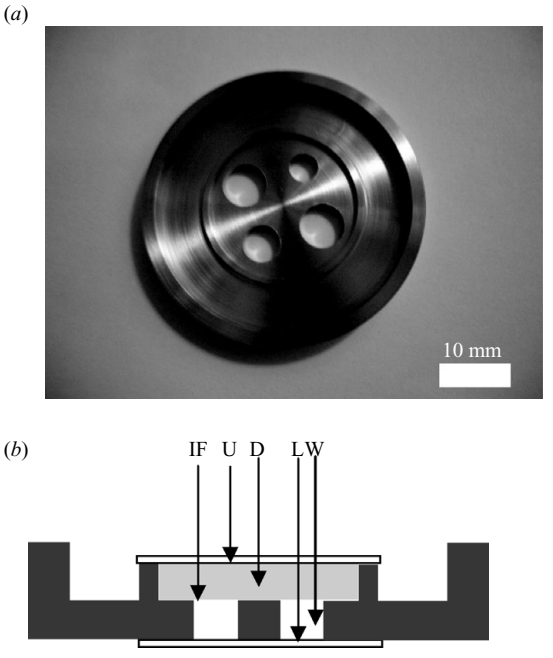

FIGURE 1. (*a*) Sample cell used to prepare a two-dimensional monolayer of colloidal particles at the decalin-water interface. (*b*) A sketch showing a cross-sectional view of the decalin–water interface: IF interface; U upper cover slip; D decalin; L lower cover slip; W water.

edge with fresh, deionized water of 18.2 M$\Omega \cdot$cm, and then add decalin to the top of the water, filling the entire height of the inner container. Another cover slip is used to cover the top of the inner container with the decalin–water interface sandwiched between the top and bottom cover slips. Figure 1(*b*) shows a cross-sectional view of the decalin–water interface made in this way. The diameter of each hole is chosen to be not too small, so that the decalin–water interface can be kept flat visually. This requirement ensures that all the interfacial particles in the view area are at the same focal plane, and they do not have a downward drift velocity due to an inclination of the interface. The diameter of each hole should also be not too large, so that the right angle of the upper sharp edge of each hole can be used to pin the water surface and reduce unwanted surface flow. Because of the non-slip boundary condition, the cover slip on the top of the fluid layers helps greatly to stabilize the interface and further reduce the interfacial flow.

Once the decalin–water interface is prepared (before the top cover slip is added to seal the sample), a small amount of precleaned concentrated PMMA/decalin solution is injected into the top decalin fluid layer. Because of density difference, the PMMA particles settle on the interface under gravity and get trapped at the interface because of capillary forces (Pieranski 1980). The coverage of PMMA particles at the interface can be readily adjusted by varying the amount of injection of the concentrated PMMA solution. In this way a well-dispersed two-dimensional monolayer of PMMA spheres is formed at the interface with both the lower (water) and upper (decalin) fluid layers of equal thickness (0.8 mm) sandwiched between the top and bottom cover slips. Great care is taken to clean the sample cell and the decalin–water interface. The stainless steel cell is cleaned in an ultrasonic bath and then washed with water for 5 minutes. A Kimwipe (280 one-ply white wipers, Kimberly–Clark) soaked with

acetone is used to further clean the cell, followed by repeat methanal and water rinses. The cleaned cell is then filled with deionized water. The water surface is aspirated to further remove residual impurities on the surface. The PMMA particles disperse well at the clean decalin–water interface. Individual particles undergo vigorous Brownian motion and remain stable at the interface for days.

The entire sample cell is placed on the sample stage of an inverted microscope (Leica DM-IRB), and the motion of the interfacial particles is viewed from below and recorded with a digital camera (CoolSnap-Pro, MediaCybernetics). Phase contrast microscopy is used to obtain good images of the particles. The spatial resolution of each image is set at 1392×1040 pixels, and each particle's cross-section occupies $\sim$30 pixels in the image. The frame rate used in the experiment varies from 1 to 10 frames per second. Commercial software (ImagePro, MediaCybernetics) with a spatial resolution of 60–100 nm is used to determine the particle positions. The particle trajectories are then constructed from the consecutive images, using homemade software, which is capable of tracking 70–80% of the particles in a typical sequence of 100 images, each containing 100 particles. Some particles are lost during the tracking because they move out of the view area. These lost particles will not affect the accuracy of the diffusion measurements. Typically, we use 10 image sequences, each containing 100 images, to calculate MSD, and the result is further averaged over repeated runs (10–20 runs). This corresponds to an average over 1 000 000 particles, ensuring that the statistical averaging is adequate.

Using the same image data, we also calculate the pair correlation function $g(r)$ (Behrens & Grier 2001; Chen *et al.* 2006) for each particle sample:

$$g(r) = \frac{2N(r)}{A\rho^2 2\pi r dr - \rho \sum_i^{edge} \delta A_i(r)}, \tag{2.1}$$

where $N(r)$ is the number of particle pairs at separation r in each image; $2\pi r dr$ is the bin area; ρ is the number density of the particles in the image; and A is the area of the image. The last term in the denominator accounts for corrections due to the edge effect, where $\delta A_i(r)$ is the missing bin area of the ith particle for large values of r outside the image.

3. Experimental Results

3.1. *PMMA*1 *spheres* ($d = 1.19$ μm)

Figure 2 shows an optical image of PMMA1 particles at the decalin–water interface. Under phase contrast microscopy, the particles appear as clear circles with uniform size distribution. These particles remain in focus under high magnification, indicating that PMMA1 spheres are closely bound to the interface, and their vertical position is determined by an energy minimum, much larger than k_BT, which keeps them at the interface (Pieranski 1980). Dinsmore *et al.* (2002) have shown, and we have independently verified, the formation of colloidosomes by the self-assembly of PMMA particles on the spherical interface of emulsion droplets of water in decalin. Such formation of PMMA-particle-stabilized emulsions further demonstrates that the PMMA spheres are bound to the interface by a large surface energy gain but not by their own weight (gravitational energy). The characteristic surface energy for the interfacial particles scales in the manner $\pi a^2\gamma$ (Pieranski 1980), which is $10^7 k_BT$ for a typical oil–water interface of interfacial tension $\gamma \approx 50$ mN/m. The surface energy remains $10^2 k_BT$ even when the particle's contact area at the interface is reduced to 10 nm^2. This value is still very large compared with the gravitational

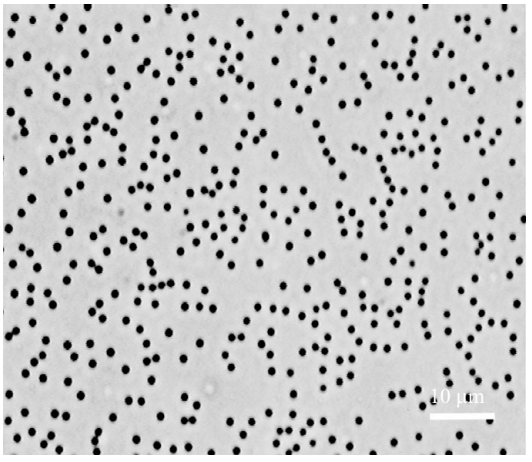

FIGURE 2. Equilibrium configuration of PMMA1 particles ($d = 1.19$ μm) at the decalin–water interface with area fraction $n \simeq 0.08$.

energy $\Delta mga \simeq 0.4k_BT$ for a PMMA1 sphere of radius a and buoyant mass Δm, where g is the gravitational acceleration. Using confocal fluorescence microscopy, Leunissen et al. (2007) showed that the PMMA particles sit very near the interface on the decalin side but not in the interface, leading to a contact angle close to 180°.

Figure 3(*a*) shows the measured pair correlation function $g(r)$ of PMMA1 particles at three area fractions. The measured $g(r)$ is zero when the interparticle distance r is smaller than the particle diameter d and approaches unity when $r \gtrsim 1.5d$. For dilute particle concentrations, $g(r)$ is related to the interaction potential $U(r)$ through the Boltzmann factor $g(r) = \exp[-U(r)/k_BT]$. The resulting $U(r)/k_BT$ at $n = 0.015$ is shown in figure 3(*b*). To avoid the crowding effect at finite concentrations, we calculate the many-body corrections to $U(r)$, using the hypernetted chain and Percus–Yevick approximations (Behrens & Grier 2001), and find that these corrections are negligible at the area fraction $n \simeq 0.015$. It is seen from figure 3(*b*) that the interaction potential for PMMA1 particles is close to that of hard spheres (dashed line) or hard disks for two-dimensional systems (Chae, Ree & Ree 1969).

As shown in figure 3(*a*), because the interaction is short-ranged, the measured $g(r)$ hardly varies when the area fraction is changed from 0.015 to 0.048. When n is increased to 0.28, the measured $g(r)$ starts to oscillate with a dominant peak at $r \simeq 1.5d$. The new length scale may reflect a small repulsive interaction between the particles, which is also visible in figure 3(*b*). An accurate imaging with fine spatial resolution is required to further resolve the amplitude and interaction range of such a small repulsion. The spatial resolution of the imaging system used in the experiment is limited, which cannot distinguish between two spheres with separation less than $r \lesssim 1.1d$. The nearly hard–sphere-like interaction shown in figure 3 assures that the short-time self-diffusion of PMMA1 particles is not be affected by their direct interactions.

Figure 4 shows the measured MSD $\langle \Delta \boldsymbol{r}^2(\tau) \rangle$ as a function of delay time τ for PMMA1 particles at two area fractions: $n = 0.014$ (circles) and $n = 0.2$ (triangles). For the small-n sample, we find that the measured $\langle \Delta \boldsymbol{r}^2(\tau) \rangle$ is a linear function of τ over the entire range of τ studied, indicating that the particles undergo free diffusion with little influence of their direct interactions. For the large-n sample, however, the measured $\langle \Delta \boldsymbol{r}^2(\tau) \rangle$ curves down slightly, as shown by the lower curve in

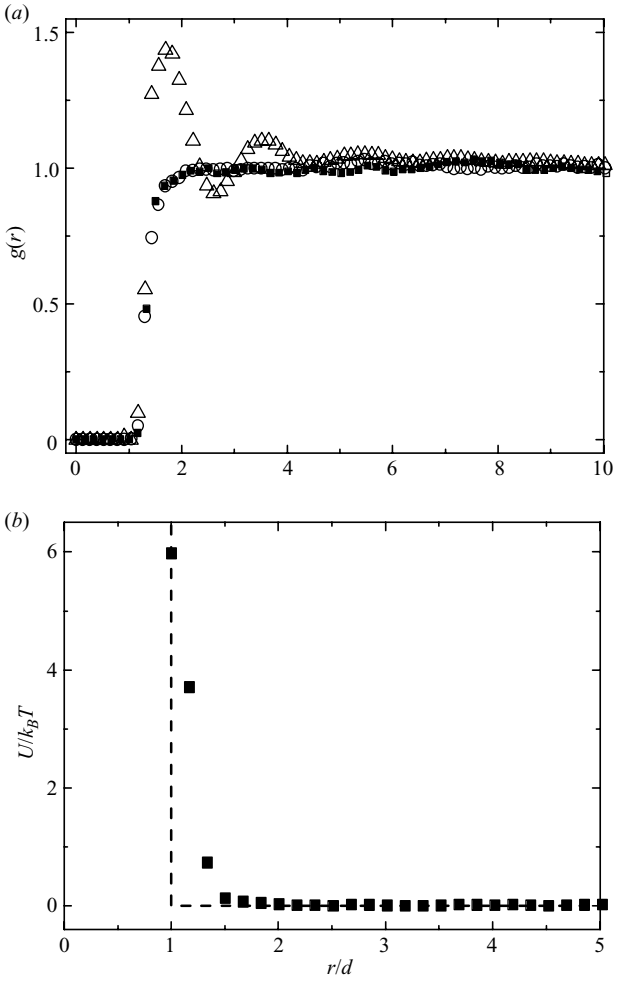

FIGURE 3. (*a*) Measured pair correlation function $g(r)$ of PMMA1 particles ($d = 1.19\,\mu$m) at three area fractions: $n = 0.015$ (solid squares); $n = 0.048$ (open circles); $n = 0.28$ (open triangles). (*b*) Normalized interaction potential $U(r)/k_BT$ (open squares) for PMMA1 particles at $n = 0.015$. The dashed line indicates the idealized interaction potential of hard spheres.

figure 4. When $n \simeq 0.2$, the mean particle separation (centre to centre) takes the value $\ell = d[\pi/(4n)]^{1/2} \simeq 2d$, suggesting that on average a tracer particle will encounter a neighbouring particle at a distance $\delta\ell = \ell - d \simeq d$. The corresponding diffusion time is $(\delta\ell)^2/D_0 = t_0 \simeq 10$ s, where $t_0 = d^2/D_0$ is the time for a particle to diffuse over its own diameter. Therefore, one expects that the Brownian motion of the interfacial particles will be hindered when $\tau \gtrsim 10$ s. Indeed, from figure 4 we find that the measured $\langle \Delta \boldsymbol{r}^2(\tau) \rangle$ starts to deviate from the linear dependence on τ when $\tau \gtrsim 10$ s.

From the initial slope of the linear fits (solid lines shown in figure 4), we obtain the short-time self-diffusion coefficient D_S^S via the equation $\langle \Delta \boldsymbol{r}^2(\tau) \rangle = 4D_S^S\tau$. Figure 5 shows how the measured $D_S^S(n)$ changes with the area fraction n for PMMA1 particles at the decalin–water interface. The measured D_S^S decreases with n, indicating an increased hindering in the particle's motion at the interface. At low surface coverage ($n \lesssim 0.2$), the measured D_S^S can be fit to a linear function, $D_S^S(n) = \alpha D_0(1 - \beta n)$ (solid

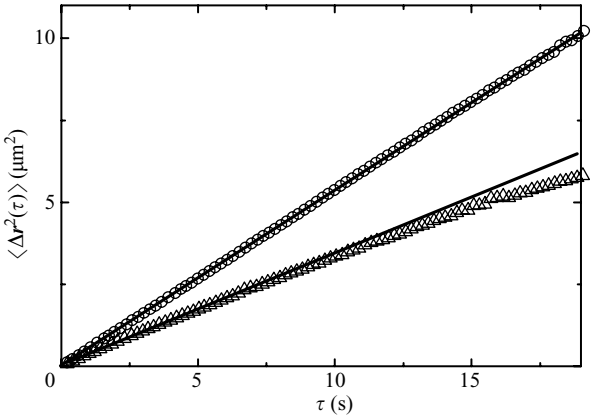

FIGURE 4. Measured mean squared displacement $\langle \Delta \boldsymbol{r}^2(\tau) \rangle$ as a function of delay time τ for PMMA1 particles ($d = 1.19\,\mu$m) at two area fractions: $n = 0.014$ (circles); $n = 0.2$ (triangles). The solid lines show the linear fit to the data points (at small τ for the lower curve).

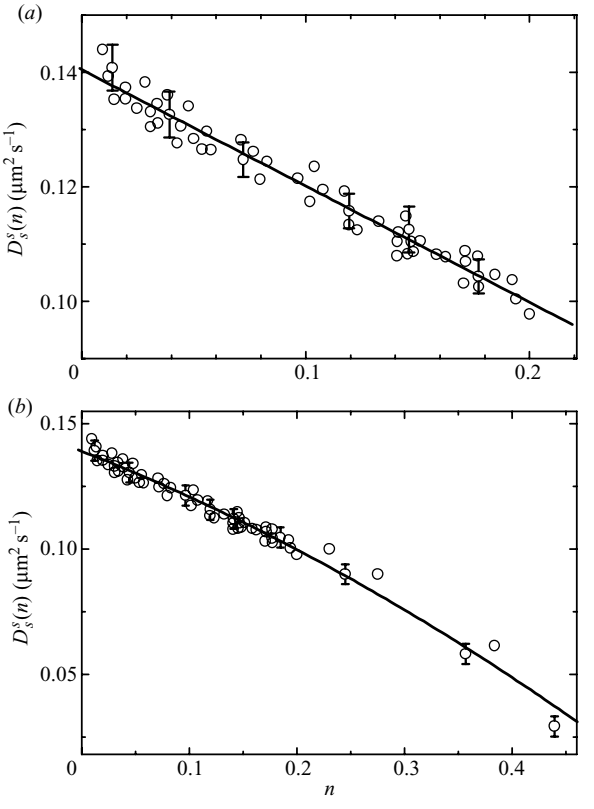

FIGURE 5. (*a*) Measured short-time self-diffusion coefficient $D_S^S(n)$ as a function of area fraction n ($n \leqslant 0.2$) for PMMA1 particles ($d = 1.19\,\mu$m) at the decalin–water interface. The solid line is a linear fit, $D_S^S(n) = 0.14(1 - 1.4n)$ (μm^2/s), to the data points. (*b*) Measured $D_S^S(n)$ vs n for PMMA1 particles over a larger span of n ($n \leqslant 0.45$). The solid line shows the second-order polynomial fit, $D_S^S(n) = 0.14(1 - 1.2n - 1.06n^2)$ (μm^{2}s^{-1}), over the entire range of n. Error bars indicate $\pm 5\%$ deviations from the mean value.

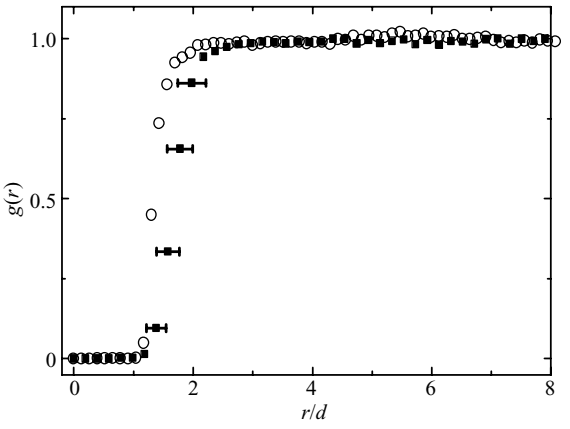

FIGURE 6. Comparison of the measured pair correlation functions $g(r)$ between PMMA2 particles ($d = 0.66\,\mu$m, solid squares) and PMMA1 particles ($d = 1.19\,\mu$m, open circles). The measurements are made at the area fraction $n = 0.01$. Error bars indicate $\pm 10\%$ deviations from the mean value.

line in figure 5*a*), with the fitted values of α and β given in table 1. The standard deviations for α are typically 7%, and those for β are 10%. The experimental uncertainties for α are mainly from statistical errors. The relatively large uncertainties for β reflect the fact that the fitted value of β also varies somewhat with the range of n chosen for the linear fit. The solid curve in figure 5(*b*) shows a second-order polynomial fit to the data points over the entire range of n studied, which gives a slightly smaller value of β. The values of α and β obtained from the second-order polynomial fit are also given in table 1.

3.2. *PMMA2 spheres* ($d = 0.66\,\mu$m)

To further verify the measured values of α and β, we repeat the short-time self-diffusion measurement for PMMA2 particles. Figure 6 compares the measured pair correlation functions $g(r)$ between PMMA2 particles (solid squares) and PMMA1 particles (open circles) at $n = 0.01$. The measured $g(r)$ for PMMA2 particles shows a similar nearly hard–sphere-like pair correlation function as PMMA1 particles do, but their effective hard-sphere diameter is slightly larger than their physical size d. The error bars in figure 6 indicate $\pm 10\%$ scatter, estimated from the individual curves of the measured $g(r)$. The measured $g(r)$ for PMMA2 particles has relatively large experimental uncertainties compared with that for PMMA1 particles. First, PMMA2 particles have a smaller optical contrast due to their smaller size. Because the refractive index difference between decalin and PMMA is very small, we cannot track the PMMA particles under phase contrast (and bright field), when their diameter becomes smaller than $0.5\,\mu$m. Second, experimental uncertainties in the separation of two nearby particles, due to the overlap of their optical images, become severer for smaller particles because of the relatively large interference effect. Finally, by watching the motion of PMMA2 particles over a period of time, we find that while most particles remain in focus for a long period of time, a small fraction of particles ($\lesssim 5\%$) move in and out of the focal plane. As a result, images of the individual particles do not appear uniform, as shown in figure 7. This is in contrast with the majority of PMMA1 particles that remain in focus and appear as clear circles with a uniform size distribution as shown in figure 2.

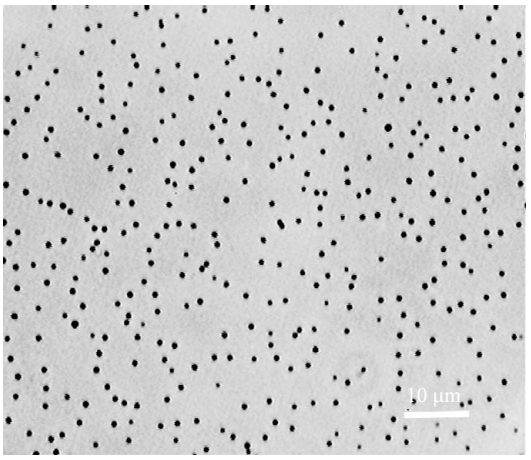

FIGURE 7. Optical image of PMMA2 particles ($d = 0.66\,\mu\text{m}$) at the decalin–water interface with area fraction $n \simeq 0.02$.

These observations indicate that the binding of PMMA2 spheres to the interface is relatively weak compared with the binding of PMMA1 spheres. As mentioned earlier, the particle's adsorption energy to the interface scales in the manner $\pi a^2\gamma$ (Pieranski 1980), which is reduced by a factor of 3.2 for PMMA2 spheres. Weak repulsions are also observed in bulk suspensions of PMMA particles dispersed in organic solvents, such as a density- and reflective-index-matched mixture of cyclohexyl bromide (CHB) and decalin (Royall, Leunissen & van Blaaderen 2003; Yethiraj & Van Blaaderen 2003). While the exact mechanisms responsible for the charging of the PMMA spheres are not known at present, it has been proposed that the origin of the charge is related to either the CHB solvent (Royall *et al.* 2003; Leunissen *et al.* 2007) or the PHSA coating on the PMMA sphere when it is in contact with water (Auer, Poon & Frenkel 2003; Schofield 2008). Apparently, the immiscible water phase acts as a 'sink' for counter-ions, which drastically increases the screening length in the oily solvent (Leunissen *et al.* 2007). The separation of micro-ions (charged PMMA spheres) and counter-ions on each side of the interface can produce anisotropic dipolar attractions between the interfacial particles (Chen *et al.* 2005; Chen *et al.* 2006; Yethiraj & Van Blaaderen 2003), which could be the cause for the occasional appearance of transient particle strings visible in figures 2 and 7. It should be emphasized that because the amount of charges on the PMMA spheres is small, the charge effects discussed earlier are rather weak, and we have not studied them systematically in this experiment. These complications in particle interaction only affect the measured $g(r)$ near the contact (and hence the corresponding high-concentration behaviour of the colloidal samples) and have little effect on the short-time self-diffusion measurements in the concentration range studied here.

Figure 8 shows the measured MSD $\langle \Delta \boldsymbol{r}^2(\tau) \rangle$ as a function of delay time τ for PMMA2 particles at two area fractions: $n = 0.008$ (circles) and $n = 0.058$ (triangles). Because the diffusion time for a PMMA2 sphere to encounter a neighbouring particle is larger than the range of delay time τ studied here, all the measured $\langle \Delta \boldsymbol{r}^2(\tau) \rangle$ show a linear dependence on τ, indicating that PMMA2 spheres undergo free diffusion with little influence of their direct interactions.

From the slope of the linear fits (solid lines shown in figure 8), we obtain the short-time self-diffusion coefficient D_S^S for PMMA2 particles. Figure 9 shows the measured

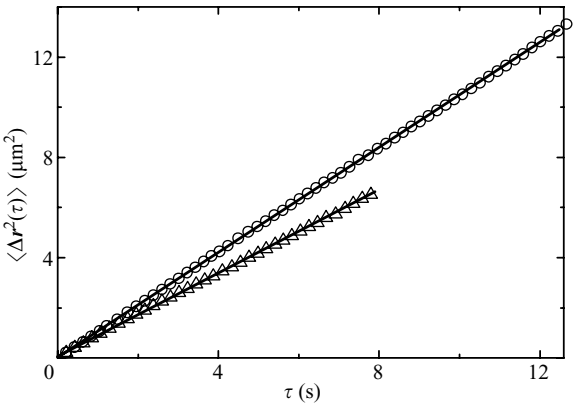

FIGURE 8. Measured mean squared displacement $\langle \Delta \boldsymbol{r}^2(\tau) \rangle$ as a function of delay time τ for PMMA2 particles ($d = 0.66$ μm) at two area fractions: $n = 0.008$ (circles); $n = 0.058$ (triangles). The solid lines show the linear fits to the data points.

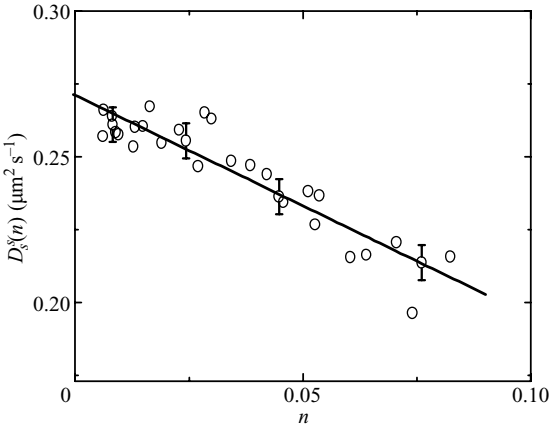

FIGURE 9. Measured short-time self-diffusion coefficient $D_S^S(n)$ as a function of area fraction n for PMMA2 particles ($d = 0.66$ μm) at the decalin–water interface. The solid line is a linear fit, $D_S^S(n) = 0.27(1 - 2.8n)$ (μm^{2}s^{-1}), to the data points. Error bars indicate $\pm 5\%$ deviations from the mean value.

$D_S^S(n)$ as a function of area fraction n for PMMA2 particles at the decalin–water interface. For the entire range of n studied here ($n \lesssim 0.08$), the measured D_S^S can be fit to a linear function, $D_S^S(n) = \alpha D_0(1 - \beta n)$, with the fitted values of α and β given in table 1. Similar to the situation for PMMA1 particles, the standard deviations for α are typically 7%, and those for β are 10%.

4. Discussion

Figures 5 and 9 reveal two novel features of interfacial hydrodynamics. First, at the single-particle level, the measured D_S^S for PMMA1 and PMMA2 particles at the $n \to 0$ limit is directly related to the drag coefficient ξ via the equation $D_S^S(n = 0) = k_B T/\xi$. For spherical particles fully immersed in a liquid of viscosity η, we have $\xi = 6\pi\eta a$

(Berne & Pecora 1976). For particles at a distance z from the interface, one finds (Radoev *et al.* 1992; Fischer *et al.* 2006)

$$\xi = (\eta_1 a) f(z/a, B), \tag{4.1}$$

where z is defined as the distance between the sphere's north pole and the interface (i.e. $z=0$ when the sphere is in contact with the interface from below), and the Boussinesq number B is defined as $B=\eta_s/[(\eta_1+\eta_2)a]$, where η_s is the shear viscosity of the interface, and η_1 and η_2 are, respectively, the viscosities of the lower and upper phase fluids forming the interface. The correction factor $f(z/a, B)$ accounts for all the effects of the interfacial hydrodynamics at the single-particle level and thus is a key quantity for understanding the rheological properties of liquid–liquid interfaces. In a recent calculation, Fischer *et al.* (2006) showed that $f(z/a, B)=k^{(0)}+k^{(1)}B+o(B^2)$, where $k^{(0)}$ and $k^{(1)}$ are two coefficients which are determined solely by the normalized distance z/a. At the $z/a\to\infty$ limit, one obtains $k^{(0)}=6\pi$ and $k^{(1)}=0$.

Using the same equations of motion and numerical procedures as described in Fischer *et al.* (2006), we calculate $f(z/a, B)$ for the decalin–water interface at 22.5°C with $\eta_1\simeq 0.96$ cP, $\eta_2=2.5$ cP, and thus $\eta_2=2.61\eta_1$. Figure 10(*a*) shows the numerically calculated zeroth-order drag coefficient $k^{(0)}$ as a function of z/a for the decalin–water interface (circles). In the plot, $z/a=0$ indicates the tracer particle is in contact with the interface from below (water side), and $z/a=-2$ indicates the particle is in contact with the interface from above (decalin side). For comparison, we also include, in figure 10(*a*), the numerically calculated $k^{(0)}$ for symmetric membranes ($\eta_2=\eta_1$, triangles) and liquid–air interfaces ($\eta_2=0$, diamonds), which have been obtained previously (Fischer *et al.* 2006). Because of the difference in symmetry, the three curves show different asymptotic behaviours. As the tracer particle moves upward from the water side (low viscosity) to the decalin side (high viscosity), the calculated $k^{(0)}$ increases smoothly from a value slightly larger than 6π (i.e. $k^{(0)}\simeq 1.58(6\pi)$ at $z/a=0$) to a value very close to $6\pi(\eta_2/\eta_1)$ (i.e. $k^{(0)}\simeq 0.974(6\pi\eta_2/\eta_1)\simeq 47.9$ at $z/a=-2$). The solid line shows the function, $k^{(0)}=29.49-14.95(z/a)-2.90(z/a)^2$, fitted to the circles. The calculated $k^{(0)}$ for the symmetric membrane (triangles) does not change much in the entire range of z/a, and its value at $z/a=-1$ is slightly larger than that when moving to either side. The calculated $k^{(0)}$ for the liquid–air interface (diamonds) decreases continuously when the tracer particle moves upward towards the air side, until it reaches its asymptotic value of zero when the particle is completely in air.

Figure 10(*b*) shows the numerically calculated first-order drag coefficient $k^{(1)}$ as a function of z/a for the decalin–water interface (circles), symmetric membranes (triangles) and liquid–air interfaces (diamonds). The calculated $k^{(1)}$ for the symmetric membrane is maximal when the particle is symmetrically immersed in both phases with its equator coinciding with the membrane plane. The calculated $k^{(1)}$ for the decalin–water interface shows a similar behaviour but with its maximum position shifted from the equatorial position ($z/a=-1$) to the side of the less viscous phase (water). The calculated $k^{(1)}$ for the liquid–air interface increases continuously when the particle moves upward towards the air side.

We now compare the calculated drag coefficients with the measurements. Because the decalin–water interface is thoroughly cleaned in the experiment, we expect the Boussinesq number B to be small in our case. Therefore, the first-order correction term, $k^{(1)}B$, is negligible. From table 1 one finds that within the experimental uncertainties, the measured $D_S^S(n=0)$ at the interface for both PMMA samples is equal to the Stokes–Einstein value D_0 in decalin. This suggests that the measured drag coefficient for both PMMA samples is $\xi\simeq 6\pi\eta_2 a$ or $k^{(0)}\simeq 6\pi(\eta_2/\eta_1)$. Comparing

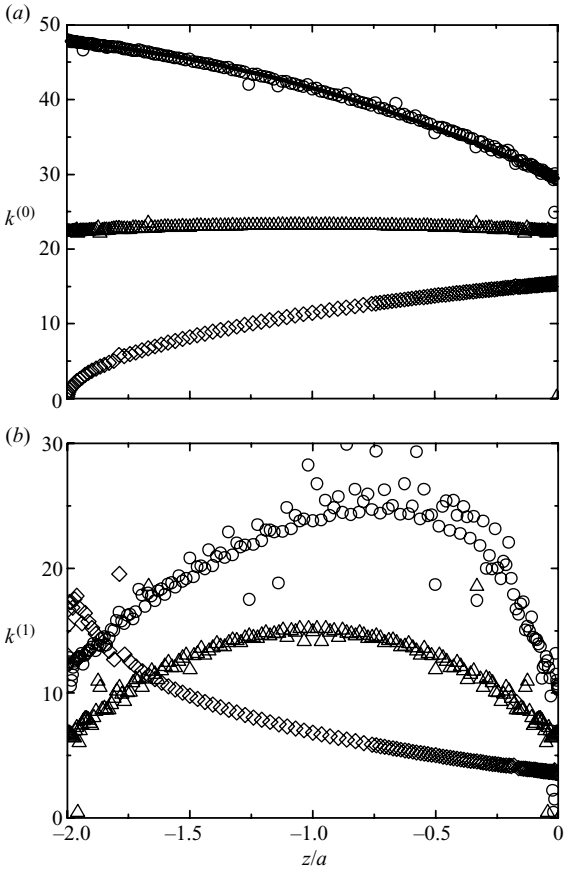

FIGURE 10. (*a*) Numerically calculated zeroth-order drag coefficient $k^{(0)}$ as a function of the normalized distance z/a for the decalin–water interface ($\eta_2 = 2.61\eta_1$, circles), symmetric membranes ($\eta_2 = \eta_1$, triangles) and liquid–air interfaces ($\eta_2 = 0$, diamonds). The solid line shows the fitted function, $k^{(0)} = 29.49 - 14.95(z/a) - 2.90(z/a)^2$. (*b*) Numerically calculated first-order drag coefficient $k^{(1)}$ as a function of z/a for the decalin–water interface ($\eta_2 = 2.61\eta_1$, circles), symmetric membranes ($\eta_2 = \eta_1$, triangles) and liquid–air interfaces ($\eta_2 = 0$, diamonds).

this result with figure 10(*a*), one immediately concludes that the vertical position of the PMMA particles relative to the interface is at $z/a \simeq -2$; i.e. the particles barely touch the interface from the decalin side. In a separate experiment, Leunissen *et al.* (2007) found that the PMMA particles do not wet the water phase, and their macroscopic contact angle at the decalin–water interface is nearly 180°. Our measurements together with the numerical calculation shown in figure 10(*a*) confirm this contact angle.

It should be noted that the calculated $k^{(0)}$ shown in figure 10(*a*) is obtained with the boundary condition that the interface be incompressible. This boundary condition is fully justifiable for interfaces with a surfactant monolayer (Fischer *et al.* 2006; Sickert *et al.* 2007) and for biological membranes (Saffman & Delbrück 1975; Saffman 1976; Stone & Ajdari 1998). In this experiment, we did not add any surfactant at the interface, and great care was taken to clean the interface and particle samples. The fitted value of α (and β) for each particle sample was extrapolated from 15–25 independent measurements conducted at different times with separately prepared decalin–water interfaces. Nevertheless, we do not have direct knowledge of whether the interface is free of contaminations, nor do we have an independent means to

quantify how clean the interface is. Levich (1962) has shown that on small length scales, residual traces of surfactant are sufficient to create significant Marangoni forces and render a free surface incompressible. Such extreme sensitivity to surface contaminations was found in the study of the motion of air bubbles rising in a viscous fluid (Bel Fdhila & Duineveld 1996; Wu & Gharib 2002). Our measurements of interfacial diffusion together with the independent contact-angle measurement appear to be consistent with the numerical calculation, assuming the decalin–water interface is incompressible.

The second new feature shown in figures 5 and 9 is that the measured values of $D_S^S(n)$ for both PMMA1 and PMMA2 particles show an interesting concentration dependence, which is directly related to the interfacial hydrodynamic interactions (IHI) between the particles. The fitted values of β for the two PMMA samples are not the same, with the larger particles having a smaller value of β. The difference between the two fitted values of β is clearly beyond the experimental uncertainties. In a separate experiment, Chen & Tong (2008) measured $D_S^S(n)$ for three silica particle samples of different sizes at a water–air interface. They found that the fitted values of β for the silica spheres also decrease with increasing particle diameter d. These results suggest that the normalized short-time self-diffusion coefficient D_S^S/D_0 at the interface depends on both n and d. The additional d dependence of the measured D_S^S/D_0 appears to be a general feature of interfacial diffusion.

For bulk (three-dimensional) colloidal suspensions, it was found that $D_S^S/D_0 = 1 - \beta_3\phi$ (Van Megan *et al.* 1987; Qiu *et al.* 1990), where ϕ is the volume fraction of particles, and the coefficient $\beta_3 \simeq 1.83$ is independent of particle size d. The measured value of β_3 agrees well with the detailed calculation of two-body hydrodynamic interactions in the bulk suspension (Qiu *et al.* 1990; Pusey 1991; Van Blaaderen *et al.* 1992; Segre *et al.* 1995). One may have a simple estimate of β_3 by examining the concentration dependence of the effective viscosity $\eta_{eff} = \eta(1 + \beta_3'\phi)$, of the colloidal suspension, where η is the solvent viscosity. Assuming $\xi \simeq 6\pi\eta_{eff}a$, one immediately obtains $D_S^S/D_0 \propto (1 - \beta_3'\phi)$. Einstein showed that $\beta_3' = 5/2$ (Russel, Saville & Schowalter 1989), which is slightly larger than the measured $\beta_3 \simeq 1.83$. This is because η_{eff} refers to the bulk (macroscopic) viscosity of the suspension, which is different from the local (microscopic) viscosity felt by a tracer particle in a bath of many particles of the same size. The local viscosity felt by the tracer particle is less than η_{eff} (Tong *et al.* 1997; Ye, Tong & Fetters 1998).

Compared with the bulk suspensions, hydrodynamic interactions between interfacial particles are much less understood. At the moment we are not aware of any theoretical calculation for β at interfaces. The motion of the colloidal monolayer is complicated because it is a coupled system of the interface with the lower and upper fluid phases. Although the contact area of the PMMA spheres at the interface is small, and the particles feel approximately the same drag as in the bulk suspension ($\alpha \simeq 1$), the influence of the interface clearly shows up in the concentration dependence of the measured D_S^S. The extra d dependence of the measured β suggests that smaller particles experience a larger resistance (dissipation) than larger particles. Such an effect was also observed in a different colloidal monolayer system consisting of weakly charged silica spheres at the water–air interface (Chen & Tong 2008) with a contact angle of $\sim 60^0$ (Tolnai 2003); i.e. approximately three fourths of the particle (by diameter) is immersed in water. An intriguing question arises from the above observations: what causes the d dependence of the measured β? Currently, there is no analytical theory or numerical simulation available to explain the effect. From the

experimental point of view, there are several candidates which may explain why large and small particles feel different hydrodynamic interactions at the interface.

One possibility is that the large and small particles may have slightly different wetting conditions at the interface. For example larger particles are bound more strongly to the interface than smaller particles. In the experiment, we also found that it gets increasingly difficulty to disperse small particles ($<0.4\,\mu m$) at the interface. Figure 6 shows that PMMA1 and PMMA2 particles experience slightly different repulsive interactions. This slight short-range repulsion could increase the effective area fraction n, making the value of the effective β smaller. This issue of interaction is further complicated if one considers that the PMMA spheres are slightly charged and that the counter-ions are distributed in the water phase near the contact point at the interface. While these effects may be very small for the equilibrium properties, such as the pair correlation function and the contact angle, of the colloidal monolayer, the dynamic properties, such as the measured D_S^S, of the monolayer could be more sensitive to these small variations. As mentioned earlier, because the relevant surface energy is large, a small change in contact area may result in a huge change in the surface energy (and hence the dissipation), much larger than k_BT.

Another possibility comes from the suspected surface contaminations mentioned earlier. While we have tried the best we could to clean the interface, we do not have direct knowledge of whether our cleaning is perfect. At the single-particle level, surface contaminations are taken care of with the boundary condition that the interface be incompressible. At the two-particle level, non-perfect cleaning may give rise to a non-zero Boussinesq number B, providing another channel for viscous dissipation (or drag). Similar to a surfactant monolayer, a monolayer of colloidal particles can also produce an effective shear viscosity, η_c, at the interface and hence give rise to an effective Boussinesq number $B_{eff} = \eta_c/[(\eta_1 + \eta_2)a]$. The value of B_{eff} is expected to increase linearly with the particle area fraction n for small values of n ($B_{eff} \simeq \beta_2 n$), and thus the drag coefficient ξ shown in 4.1 takes the form $\xi \simeq \eta_1 a(k^{(0)} + k^{(1)}\beta_2 n)$. This renormalized form of $\xi(n)$ can explain the n dependence of the measured $D_S^S(n) = k_BT/\xi(n)$. Complicated geometry effects, such as those discussed earlier and the particle size dependence of the measured β, are presumably contained in the two proportionality constants $k^{(1)}$ and β_2. Clearly, a detailed calculation of two-body hydrodynamic interactions at the interface is needed in order to fully understand the concentration dependence of the measured $D_S^S(n)$.

5. Conclusion

We have carried out a systematic study of short-time self-diffusion of monodisperse polymethylmethacrylate (PMMA) spheres at a decalin–water interface. This is a model two-dimensional system, in which the PMMA particles interact nearly like hard spheres. Two particle sizes are used in the experiment: one has diameter $d = 1.19\ \mu m$, and the other has $d = 0.66\ \mu m$. An important objective of the paper is to delineate the experimental conditions and procedures, including cleaning of the interface and purification of the colloidal samples, under which one can obtain accurate and reliable data for the short-time self-diffusion coefficient D_S^S. Optical microscopy and multi-particle tracking are used to measure $D_S^S(n)$ as a function of the area fraction n occupied by the interfacial particles. It is found that the measured D_S^S at low surface coverage has the form $D_S^S(n) = \alpha D_0(1 - \beta n)$, where D_0 is the Stokes–Einstein diffusion coefficient for the bulk suspension of PMMA spheres in decalin. The measured values of α for both PMMA samples are close to unity. The measured values of β for the

two PMMA samples are not the same with the larger particles having a smaller value of β (see table 1).

The measured $D_S^S(n)$ in the dilute limit ($n \to 0$) is directly related to the single-particle drag coefficient ξ at the interface. Using the equation $D_S^S(n=0) = k_B T/\xi$ and the measured value of $\alpha \simeq 1$, we find $\xi \simeq 6\pi\eta_2 a$, where η_2 is the viscosity of decalin. This result together with the early confocal microscope observations (Leunissen *et al.* 2007) that the PMMA particles sit very near the interface on the decalin side confirm the numerical calculation of the zeroth-order drag coefficient $k^{(0)}$ shown in figure 10(*a*). The measured single-particle self-diffusion at the interface together with the calculated drag coefficient thus provide an accurate method to determine the contact angle of colloidal particles at the interface. The concentration dependence of the measured $D_S^S(n)$ is caused by hydrodynamic interactions between the particles at the interface. The measured particle-size dependence of the linear coefficient β is a new feature of interfacial diffusion, which is absent from three-dimensional diffusion in bulk suspensions. Currently, there is no analytical theory or numerical simulation available to explain the origin of the measured particle-size dependence of β. Several scenarios are discussed from the experimental point of view in § 4, but a more quantitative understanding about the concentration dependence of $D_S^S(n)$ requires a detailed calculation of two-body hydrodynamic interactions at the interface.

We have benefited from illuminating discussions and correspondence with H. Stone, M. Brenner, A. Schofield, B. Ackerson, T. Squires and A. Levine. PT was supported by the Research Grants Council of Hong Kong SAR under grant no. HKUST603305. TMF acknowledges support from the US National Science Foundation (NSF) under CHE-0649427, and DAW acknowledges NSF for support under DMR-0602684.

REFERENCES

Antl, L., Goodwin, J. W., HIill, R. D., Ottewil, R. H., Owens, S. M. & Papworth, S. 1986 The preparation of polymethyl methacrylate latices in non-aqueous media. *Colloids Surf.* **17**, 67.

Auer, S., Poon, W. C. K. & Frenkel, D. 2003 Phase behaviour and crystallization kinetics of poly-12-hydroxystearic-coated polymethylmethacrylate colloids. *Phys. Rev.* E **67** (1–4), 020401.

Bausch, A. R., Bowick, M. J., Cacciuto, A., Dinsmore, A. D., Hsu, M. F. & Nelson, D. R., Nikolaides, M. G., Travesset, A. & Weitz, D. A. 2002 Grain boundary scars and spherical crystallography. *Science* **299**, 1716–1718.

Behrens, S. H. & Grier, D. G. 2001 Pair interaction of charged colloidal spheres near a charged wall. *Phys. Rev.* E **64** (1–4), 050401.

Bel Fdhila, R. & Duineveld, P. C. 1996 The effect of surfactant on the rise of a spherical bubble at high Reynolds and Péclet numbers. *Phys. Fluids* **8**, 310–321.

Berne, B. J. & Pecora, R. 1976 *Dynamic Light Scattering*. Wiley.

Binks, B. P. 1998 *Modern Aspects of Emulsion Science*. Royal Society of Chemistry.

Chae, D.-G., Ree, F. H. & Ree, T. 1969 Radial distribution functions and equation of state of the hard-disk fluid. *J. Chem. Phys.* **50**, 1581–1589.

Chen, W., Tan, S.-S., Ng, T.-K., Ford, W. T. & Tong, P. 2005 Long-ranged attraction between charged polystyrene spheres at aqueous interfaces. *Phys. Rev. Lett.* **95** (1–4), 218301.

Chen, W., Tan, S.-S., Ng, T.-K., Ford, W. T. & Tong, P. 2006 Measured long-ranged attractive interaction between charged polystyrene latex spheres at a water–air interface. *Phys. Rev.* E **74** (1–14), 021406.

Chen W. & Tong, P. 2008 Short-time self-diffusion of weakly charged silica spheres at aqueous interfaces. *Euro. Phys. Lett.* **84**, 28003.

Dahan, M., Levi, S., Luccardini, P., Rostaing, C., Riveau, B. & Triller, A. 2003 Diffusion dynamics of Glycine receptors revealed by single-quantum dot tracking. *Science* **302**, 442–443.

Danov, K., Aust, R., Durst, F. & Lange, U. 1995 Influence of the surface viscosity on the hydrodynamic resistance and surface diffusivity of a large Brownian particle. *J. Colloid Interface Sci.* **175**, 36–45.

Dimova, R., Danov, K., Pouligny, B. & Ivanov, I. B. 2000 Drag of a solid particle trapped in a thin film or at an interface: influence of surface viscosity and elasticity. *J. Colloid Interface Sci.* **226**, 35–43.

Dinsmore, A. D., Hsu, M. F., Nikolaides, M. G., Marquez, M., Bausch, A. R. & Weitz, D. A. 2002 Colloidosomes: selectively permeable capsules composed of colloidal particles. *Science* **298**, 1006–1009.

Fernández-Toledano, J. C., Moncho-Jordá, A., Martinez-López, F. & Hidalgo-Álvarez, R. 2004 Spontaneous formation of mesostructures in colloidal monolayers trapped at the air–water interface: a simple explanation. *Langmuir* **20**, 6977–6980.

Fischer, T. M. 2004 Comment on 'shear viscosity of Langmuir monolayers in the low-density limit'. *Phys. Rev. Lett.* **92**, 139603.

Fischer, T. M., Dhar, P. & Heinig, P. 2006 The viscous drag of spheres and filaments moving in membranes or monolayers. *J. Fluid Mech.* **558**, 451–475.

Helmer, M. 2005 Surfaces and interfaces. *Nature* **437**, 637–637.

Hurd, A. J. & Shaefer, D. W. 1985 Diffusion-limited aggregation in two dimensions. *Phys. Rev. Lett.* **54**, 1043–1046.

Kollmann, M., Hund, R., Rinn, B., Nägele, G., Zahn, K., König, H., Maret, G., Klein R. & Dhont, J. K. G. 2002 Structure and tracer-diffusion in quasi-two-dimensional and strongly asymmetric magnetic colloidal mixtures. *Europhys. Lett.* **58**, 919–925.

Leunissen, M. E., Van Blaaderen, A., Hollingsworth, A. D., Sullivan, M. T. & Chaikin, P. M. 2007 Electrostatics at the oil–water interface, stability, and order in emulsions and colloids. *PNAS* **104**, 2585–2590.

Levich, V. G. 1962 *Physicochemical Hydrodynamics.* Prentice Hall.

Lipowsky, P., Bowick, M. J., Meinke, J. H., Nelson, D. R. & Bausch, A. R. 2005 Direct visualization of dislocation dynamics in grain-boundary scars. *Nat. Mater.* **4**, 407–411.

Nikolaides, M. G., Bausch, A. R., Hsu, M. F., Dinsmore, A. D., Brenner, M. P., Gay, C. & Weitz, D. A. 2002 Electric-field-induced capillary attraction between like-charged particles at liquid interfaces. *Nature* **420**, 299–301.

Onada, G. Y. 1985 Direct observation of two-dimensional, dynamic clustering and ordering with colloids. *Phys. Rev. Lett.* **55**, 226–229.

Pieranski, P. 1980 Two-dimensional interfacial colloidal crystals. *Phys. Rev. Lett.* **45**, 569–572.

Prasad, V., Koehler, S. A. & Weeks, E. R. 2006 Two-particle microrheology of quasi-two-dimensional viscous systems. *Phys. Rev. Lett.* **97** (1–4), 176001.

Pusey, P. N. 1991 In *Liquids, Freezing and Glass Transition* (ed. J.-P. Hansen, D. Levesque & J. Zinn-Justin), chapter 10. North-Holland.

Qiu, X., Wu, X. L., Xue, J. Z., Pine, D. J., Weitz D. A. & Chaikin, P. M. 1990 Hydrodynamic interactions in concentrated suspensions. *Phys. Rev. Lett.* **65**, 516–519.

Radoev, B., Nedjalkov, M. & Djakovich, V. 1992 Brownian motion at liquid–gas interfaces. Part 1. Diffusion coefficients of macroparticles at pure interfaces. *Langmuir* **8**, 2962–2965.

Rinn, B., Zahn, K., Maass P. & Maret, G. 1999 Influence of hydrodynamic interactions on the dynamics of long-range interacting colloidal particles. *Europhys. Lett.* **46**, 537–541.

Royall, C. P., Leunissen, M. E. & Van Blaaderen, A. 2003 A new colloidal model system to study long-range interactions quantitatively in real space. *J. Phys.: Condens. Matter* **15**, S3581–S3596.

Russel, W. B., Saville, D. A. & Schowalter, W. R. 1989 *Colloidal Dispersion.* Cambridge University Press.

Sackmann, E. 1996 Supported membranes: scientific and practical applications. *Science* **271**, 43–48.

Saffman, P. G. 1976 Brownian motion in thin sheets of viscous fluid. *J. Fluid Mech.* **73**, 593–603.

Saffman, P. G. & Delbrück, M. 1975 Brownian motion in biological membranes. *PNAS* **72**, 3111–3113.

Schofield, A. 2007 Personal website. http://www.ph.ed.ac.uk/∼abs/.

Schofield, A. 2008 Private communication.

Segre, P. N., Behrend, O. P. & Pusey, P. N. 1995 Short-time Brownian motion in colloidal suspensions: experiment and simulation. *Phys. Rev.* E **52**, 5070–5083.

Sickert, M. & Rondelez, F. 2003 Shear viscosity of Langmuir monolayers in the low-density limit. *Phys. Rev. Lett.* **90** (1–4), 126104.

Sickert, M. & Rondelez, F. 2004 Reply. *Phys. Rev. Lett.* **92** (1), 139604.

Sickert, M., Rondelez, F. & Stone, H. A. 2007 Single-particle Brownian dynamics for characterizing the rheology of fluid Langmuir monolayers. *Euro. Phys. Lett* **79** (1–6), 66005.

Stone, H. & Ajdari, A. 1998 Hydrodynamics of particles embedded in a flat surfactant layer overlying a subphase of finite depth. *J. Fluid Mech.* **369**, 151–173.

Tolnai, G., Agod, A., Kabai-Faix, M., Kovacs, A. L., Ramsden, J. J. & Horvolgyi, Z. 2003 Evidence for secondary minimum flocculation of Stöber silica nanoparticles at the air–water interface: film balance investigations and computer simulations. *J. Phys. Chem.* B **107**, 11109–11116.

Tong, P., Ye, X., Ackerson, B. J. & Fetters, L. J. 1997 Sedimentation of colloidal particles through a polymer solution. *Phys. Rev. Lett.* **79**, 2363–2367.

Van Blaaderen, A., Peetermans, J., Maret G. & Dhont, J. K. G. 1992 Long-time self-diffusion of spherical colloidal particles measured with fluorescence recovery after photo-bleaching. *J. Chem. Phys.* **96**, 4591–4603.

Van Megan, W., Underwood, S. M., Ottewill, R. H., Williams, N. St. J. & Pusey, P. N. 1987 Particle diffusion in concentrated dispersions. Faraday Discuss. *Chem. Soc.* **83**, 47–57.

Wu, M.-M. & Gharib, M. 2002 Experimental studies on the shape and path of small air bubbles rising in clean water. *Phys. Fluids* **14**, L49–L52.

Ye, X., Tong, P. & Fetters, L. J. 1998 Transport of probe particles in semidilute polymer solutions. *Macromolecules* **31**, 5785–5793.

Yethiraj, A. & Van Blaaderen, A. 2003 A colloidal model system with an interaction tunable from hard sphere to soft and dipolar. *Nature* **421**, 513–517.

Zahn, K., Mendez-Alcaraz, J. M. & Maret, G. 1997 Hydrodynamic interactions may enhance the self-diffusion of colloidal particles. *Phys. Rev. Lett.* **79**, 175–178.